JOURNAL OF AIRCRAFT
Vol. 36, No. 3, May–June 1999

Time-History Effects on a Rolling 65-Degree Delta-Wing-Body Configuration

Lars E. Ericsson*
Mountain View, California 94040

An analysis of the experimental results for a 65-deg delta wing rolling about a 30-deg inclined axis indicates that the roll-rate-induced camber effect on vortex breakdown is associated with a significantly larger time lag than the pitch-rate-induced camber effect. A flow hypothesis is presented that can explain this difference between the two types of oscillatory motion.

Nomenclature

b = wingspan
c = wing root chord
$\bar{c}$ = mean aerodynamic chord
f = oscillation frequency
k = reduced frequency, $\omega b/2U_\infty$
l = rolling moment coefficient, $C_l = l/(\rho_\infty U_\infty^2/2)Sb$
m = pitching moment coefficient, $C_m = m/(\rho_\infty U_\infty^2/2)S\bar{c}$
$P(t)$ = flow state $[\phi(t), \dot{\phi}(t)]$
S = reference area, projected wing area
t = time
U = horizontal velocity
$\bar{U}$ = mean convection velocity
x = chordwise coordinate
α = angle of attack
Δ = increment or amplitude
θ = pitch perturbation around α_0
ξ = dimensionless x coordinate, x/c
ρ = air density
σ = inclination of the roll axis
ϕ = roll angle
$\dot{\phi}$ = roll rate
$\dot{\phi}$ = reduced roll rate, $\dot{\phi}b/2U_\infty$
ω = angular frequency, $2\pi f$
$\bar{\omega}$ = reduced frequency, $\omega c/U_\infty$

Subscripts

B = vortex breakdown
C = camber
CG = center of gravity or pitch axis location
U = upstream
V = vortex
∞ = freestream conditions
0 = trim or time-average value

Differential Symbols

C_{m_θ} = $\partial C_m/\partial\theta$
$C_{m_{\dot{\theta}}}$ = $\partial C_m/\partial(\dot{\theta}\bar{c}/U_\infty)$
$\dot{\phi}$ = $\partial\phi/\partial t$

Introduction

THE original test of a sharp-edged 65-deg delta wing[1] was intended to demonstrate that the high-alpha aerodynamics were so highly nonlinear that locally linearized methods could not be used, making the concept of stability derivatives meaningless. The test not only demonstrated this fact, but also indicated that the nonlinear aerodynamics were more complicated than what had been anticipated. The numerous tests that followed have revealed that the simple model geometry exhibits a multitude of nonlinear flow phenomena that will play important roles in high-alpha maneuvers of slender-winged agile aircraft.[2] This paper analyzes the time-history effects on the unsteady aerodynamics of a 65-deg delta-wing-body model (Fig. 1), describing roll oscillations around a 30-deg inclined body axis. It should be emphasized that the test results[1,3] were not obtained for a pure delta wing. It is shown in Ref. 4 that at $\alpha = 30$ deg and $\phi = 0$, vortex breakdown would occur forward of 15% chord on a pure delta wing, not aft of 40% chord as in the present case. Although the vortex breakdown would leave the leeside wing half at some value $|\phi| \gg 5$ deg, the critical state located at $|\phi| \approx 5$ deg could only occur at $\alpha = 30$ deg in the presence of the body-induced upwash along the leading edges of the 65-deg delta wing. For simplicity, the body is not present in the sketches of the delta wing used throughout the present paper to illustrate the effects of roll angle and roll rate on vortex breakdown.

Discussion

The experimental results[3] in Fig. 2 show unexpectedly large differences between the $C_l(\phi)$ characteristics for roll oscillations around $\phi = 0$ at different rates. As the oscillations were not expected to encounter a critical state,[5] the huge difference between the $C_l(\phi)$ characteristics was a big surprise. It is suggested in Refs. 6–9 that the likely source of the different characteristics in Fig. 2 could be differences in the magnitude of the roll-rate-induced camber effect on the dynamically equivalent steady (DES) aerodynamics, described in Ref. 10 for a pitching delta wing. The DES characteristics of a rolling delta wing are those measured in a static test with the cambered delta-wing geometry shown in the bottom sketch of the top inset in Fig. 3. The same characteristics can also be obtained by integrating the quasisteady load distribution generated by the roll-rate-induced velocity distribution shown in the middle sketch of the inset. The advantage with the DES characteristics is that they can be obtained in static tests with a suitably shaped model, as illustrated in Fig. 3. The unsteady aerodynamics are obtained by adding time-history effects to the DES aerodynamic characteristics. The rate-induced camber effect was confirmed by static tests[11] using a model with wings deformed to give the conical camber equivalent to that generated by the 65-deg delta wing during positive and negative ϕ ramps at the reduced roll rate $|\bar{\dot{\phi}}| = |\dot{\phi}b/2U_\infty| = 0.012$ (Fig. 3). The results showed that the rate-induced camber caused a shift $\Delta\xi_B \approx \pm 0.1$ at $\alpha = 30$ deg. The static tests were performed for $\phi = 0$. As discussed at length in Refs. 6–9, one expects the effect of camber to be more dramatic at ϕ values close to the critical state at $|\phi| \approx 5$ deg. The static characteristics for the undeformed wing–body configuration[12] (Fig. 4) show that when ϕ is decreased

Presented as Paper 97-3645 at the AIAA Guidance, Navigation, and Control Conference, New Orleans, LA, Aug. 11–13, 1997; received Oct. 8, 1997; revision received Dec. 29, 1998; accepted for publication Jan. 6, 1999.

*Engineering Consultant. Fellow AIAA.

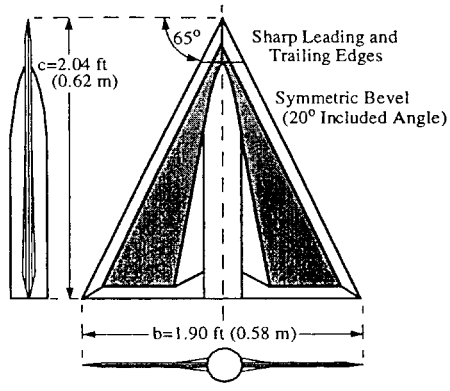

Fig. 1 Model geometry.[1]

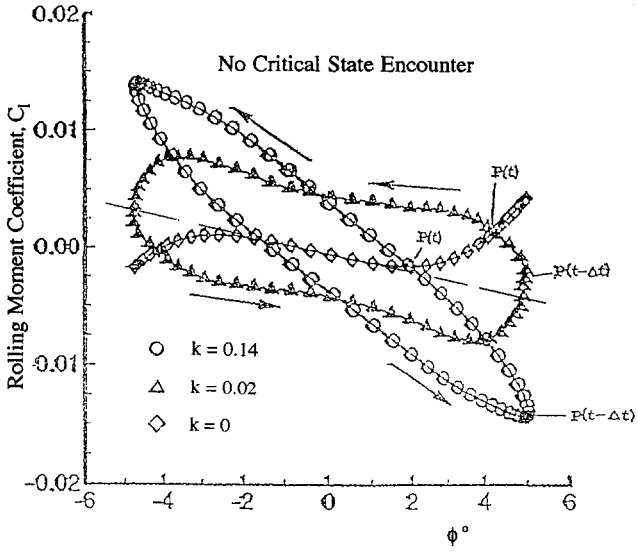

Fig. 2 $C_l(\phi)$ characteristics of 65-deg delta wing at $|\phi| \leq 5$ deg.[3]

past $\phi = -4$ deg and the critical state is approached, the breakdown movement with decreasing ϕ toward the trailing edge on the leeward wing half occurs with a greatly increased rate, causing a correspondingly rapid change of the rolling moment (Fig. 2). Performing the static test at a range of roll angles that included the critical state, as suggested in Ref. 6, should have provided the needed information about the increased effect of roll-rate-induced camber near the critical state.

At $\phi = 0$, the static rolling moment is zero, and the nonzero C_l in Fig. 2 at $\phi = 0$ for $k \neq 0$ is generated by the roll-rate-induced camber effect. The dominant effect of camber is expected to be responsible for the C_l difference between increasing and decreasing ϕ branches, even in the presence of time-history effects. However, near the ends of the $C_l(\phi)$ loops, where the roll rate changes rapidly with roll angle, the time-history effects could be very large. Initially, the author expected that the required cancellation of dynamic effects, giving the required loop intersection with the static C_l at $P(t)$ in Fig. 2, would result if $P(t - \Delta t)$ were located at the ends of the $C_l(\phi)$ loops, assuming that the roll-rate-induced camber was the dominant effect controlling the location of vortex breakdown.[9] However, this would require that the time lag Δt was different for $k = 0.02$ and 0.14.† Thus, the roll-rate-induced camber could not be the only significant effect, at least not for the determination of the intersection between dynamic and static $C_l(\phi)$ characteristics. However, the dominance of the pitch-rate-induced camber effect on a pitching 52-deg delta wing has been established[13,14] (Fig. 5). Because of the pitch-rate-induced negative angle of attack at the apex, the

† Huang, X. Z., private communicaton, 1996.

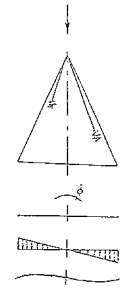

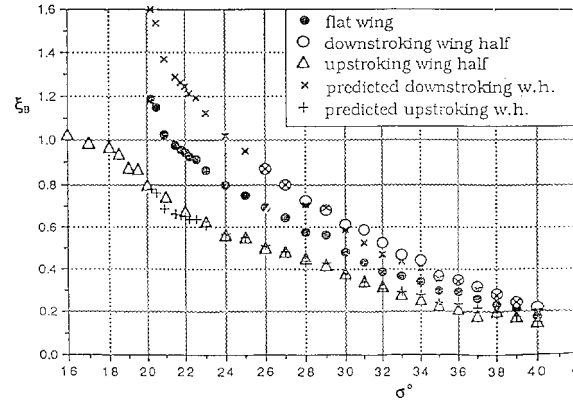

Fig. 3 Vortex breakdown location on deformed sheet-metal model simulating the roll-rate-induced camber at $\dot{\phi}$ = 0.012 (Ref. 11).

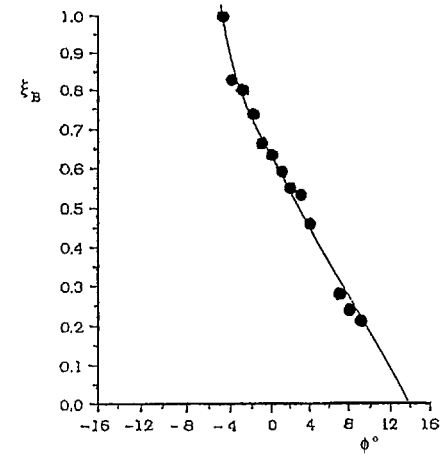

Fig. 4 Effect of roll angle on vortex breakdown at σ = 30 deg.[11]

vortex on the top side does not start to develop until $\alpha(t) \approx 16$ deg, with vortex breakdown starting at $\alpha(t) \approx 14$ deg on the backstroke. During the upstroke, the positive pitch-rate-induced camber effect $\Delta\alpha_c > 0$ (see inset in Fig. 5) will delay the occurrence of breakdown, whereas $\Delta\alpha_c < 0$ during the backstroke will promote it.[14] If one assumes that the pitch-rate-induced camber effect controls the breakdown, the most aft location of breakdown would occur when the switch at $\alpha(t) = 20$ deg from positive to negative $\Delta\alpha_c$ had been fully realized at $\xi_B \approx 0.7$. Using this information, a convection velocity for the time-history effect on the pitch-rate-induced camber was determined[14] ($\bar{U}_B \approx 0.70\bar{U}_V$, where $\bar{U}_V \approx U_\infty$). This was used to predict[15] that the maximum adverse camber effect, generated at $\alpha(t) = 10$ deg during the backstroke, would have been convected to the most forward breakdown location when $\alpha(t) = 1.8$ deg. As this was in very good agreement with the experimental results[13] (Fig. 5), it could be concluded that the pitch-rate-induced camber had a dominant effect on the vortex breakdown. The decreasing angle of attack $\alpha(t)$ on the backstroke would act counter to the pitch-rate-induced camber effect, delaying the forward motion of vortex breakdown.

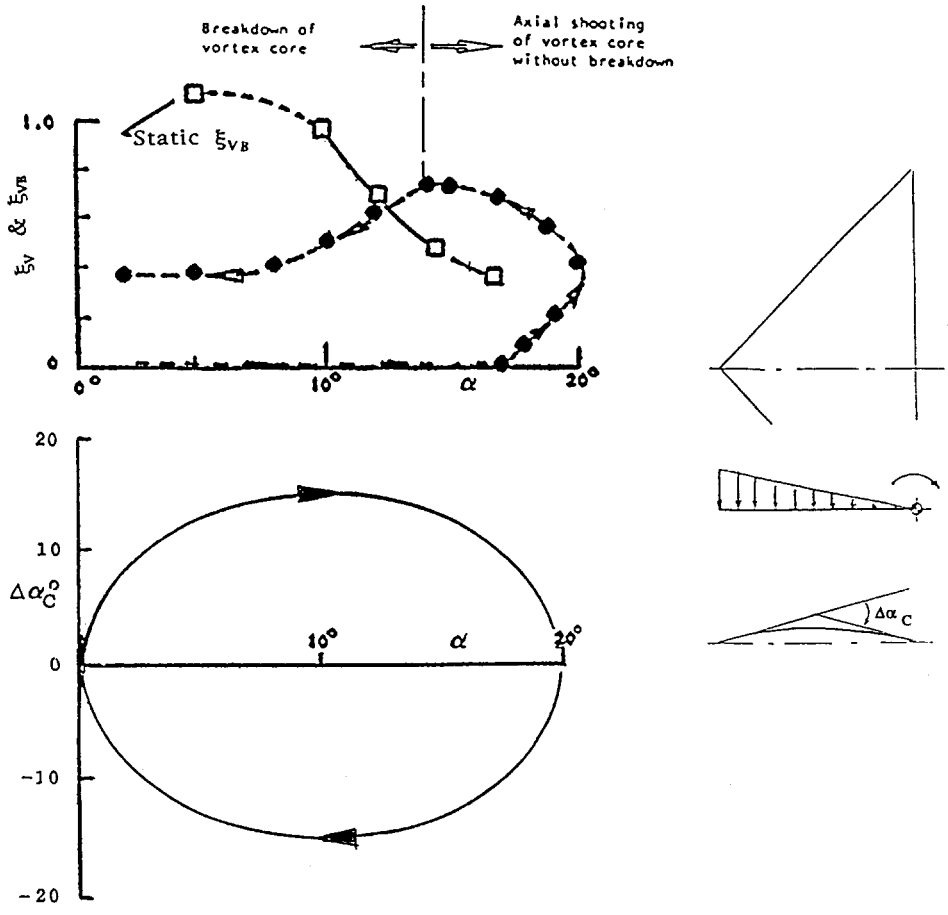

Fig. 5 Effect of pitch-rate-induced camber on the vortex breakdown on a 52-deg delta wing.[13,14]

It could, therefore, not be of significant magnitude compared with the camber effect. Thus, for a pitching delta wing, the rate-induced camber is apparently the dominant effect on vortex breakdown. Why is it that the roll-rate-induced camber effect does not appear equally dominating?

Influence of Time History on Rate-Induced Camber Effects

For the pitching delta wing, the rate-induced upwash (and downwash) is largest at the apex for rotation centers aft of midchord. In contrast, for the rolling delta wing, the rate-induced upwash (and downwash) is zero at the apex and maximum at the trailing edge. That is, for the pitching delta wing, the rate-induced camber effect is initiated at the apex, whereas for the rolling delta wing, it starts at the trailing edge. It is well recognized that on stalling airfoils the essential rate-induced effects are concentrated to the leading edge, where the initial boundary-layer development occurs.[16] Likewise, one expects that the downstream development of the leading-edge vortex on a delta wing will be strongly dependent on the initial conditions at the apex. Analysis[17] of unsteady aerodynamic results for a pitching 69.6-deg delta wing[18] indicates that this is indeed the case (Fig. 6). The prediction[17] in Fig. 6 was obtained by using the method derived for sharp-edged delta wings,[19] modified to account for the delay of crossflow separation caused by the leading-edge roundness.[20] There was apparently no significant moving wall effect[21] associated with the rounded leading edge. Because this is the dominant effect on dynamic airfoil stall,[22] the results in Fig. 6 were at first very surprising. However, the results are in agreement with the dominance of apex flow conditions on the downstream vortex development shown by Lambourne et al., and Lambourne and Bryer both in the absence[23] and presence[24] of vortex breakdown. These results were, however, obtained for sharp-edged delta wings. For the case in Fig. 6, where the leading edge is rounded and the apex is conical in shape, the

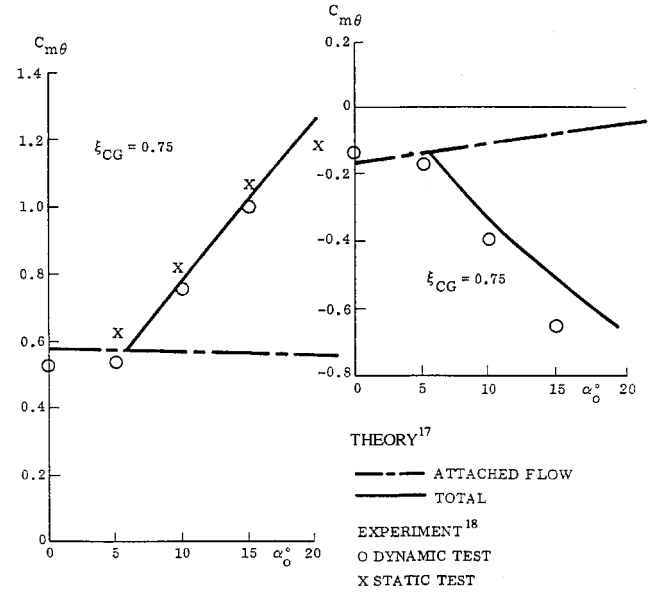

Fig. 6 Static and dynamic stability derivatives of a pitching 69.6-deg delta wing.

results for pointed bodies of revolution apply. Such results[25] show that also in this case the flow conditions at the apex determine the downstream development of the body vortices.[26,27] It follows from the preceding discussion that the roll-rate-induced camber effect must be communicated to the apex before it can effectively influence the leading-edge vortices. The associated large time-history effects prevent the power of the rate-induced camber effect from being as apparent for rolling as for pitching delta wings.

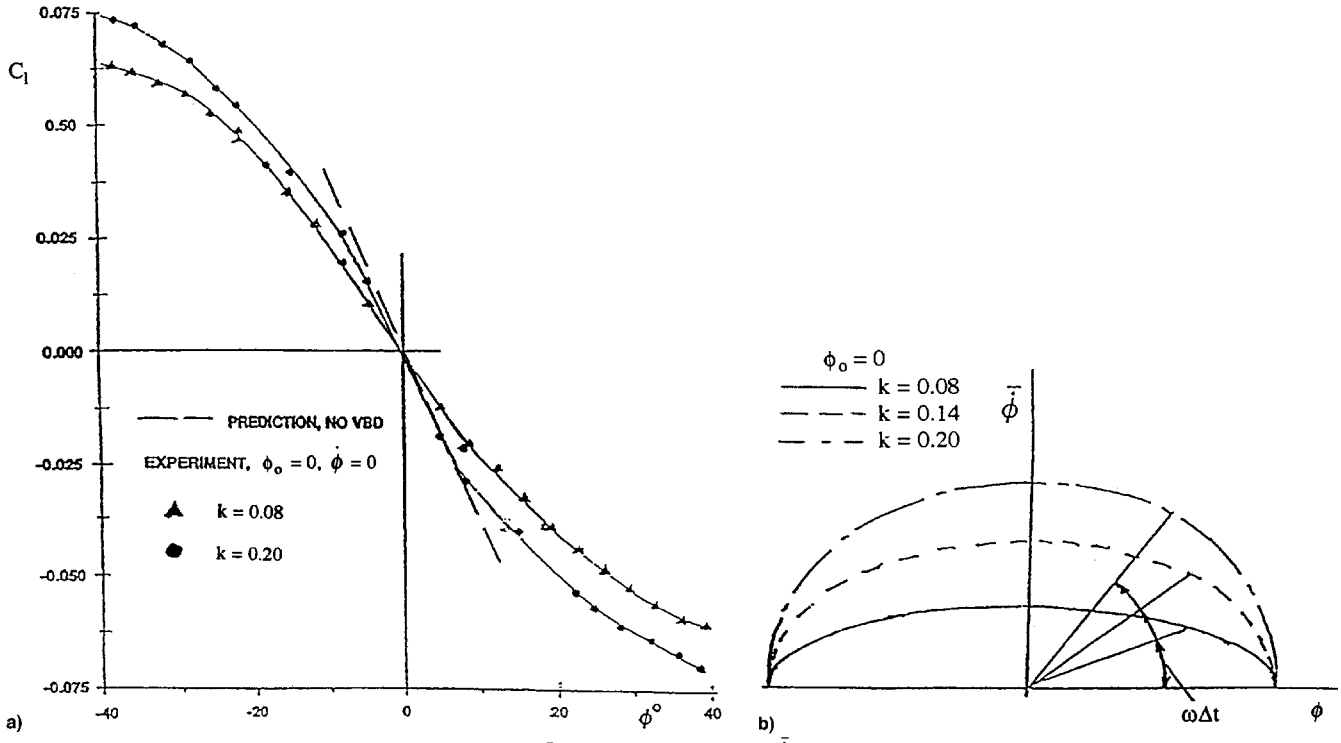

Fig. 7 Effect of roll rate on measured $C_l(\phi)$ characteristics[7]: a) $C_l(\phi)$ at $\phi_0 = 0$ and $\dot{\phi} = 0$ for various reduced frequencies, and b) effect of time lag on residual roll-rate effect at $\dot{\phi} = 0$.

When analyzing the results in Fig. 2, the conclusion was drawn[9] that the time histories of both roll angle and roll rate must have played a role in determining the intersections between the dynamic and static characteristics. The rolling moment at $\phi = 5$ deg in Fig. 2 reveals that $C_l(\phi)$ at $\phi = 0$ for $k = 0.14$ has a statically stabilizing slope that is vastly larger in magnitude than that for $k = 0$, whereas the same is not true for $k = 0.02$. That is in agreement with data trends established earlier[7] (Fig. 7). Because of the time-history effect, represented by the time-lag effect $\omega\Delta t$ in Fig. 7b, the residual rate-induced camber effect at $\dot{\phi} = 0$ is substantial. For $k = 0.20$, the $C_l(\phi)$ slope approaches that predicted in the absence of vortex breakdown[28] (Fig. 7a). This explains the large deviation of C_l for $k = 0.14$ at $\phi = \pm 5$ deg from the extension of the static slope at $\phi = 0$ in Fig. 2. Thus, the rate-induced camber effect existing at the ends of the $C_l(\phi)$ loops, where $\dot{\phi} = 0$, is far from zero for $k = 0.14$, and could, therefore, never, by itself, assure the required loop intersection of $P(t)$ with the static characteristics. In the case of $k = 0.02$, however, the residual (statically stabilizing) camber effect at $\phi = \pm 5$ deg would appear to be quite small (Fig. 7), causing the dynamic $C_l(\phi)$ slope at $\phi = 0$ in Fig. 2 to show no measurable difference from the static slope.

The contrasting shapes of the dynamic $C_l(\phi)$ loops in Fig. 2 for $k = 0.02$ and 0.14 provide significant clues about the difference in time-history effects. In the case of $k = 0.02$, the loop widens toward the ends; whereas for $k = 0.14$, the width remains roughly the same as at $\phi = 0$ until $|\phi| > 3$ deg. Even for $k = 0.02$, the time-lag effect for the rate-induced camber is apparently not insignificant, causing the maximum camber effect generated at $\phi = 0$ to be felt toward the ends of the $C_l(\phi)$ loop, producing the maximum width of the loop at $|\phi| = 3.2$ deg. For the effective time lag Δt, the maximum roll rate at $\phi = 0$ would be felt at $\phi = 3.2$ deg when $\omega\Delta t = \sin^{-1}(3.2/5) = 40$ deg. As this phase lag $\omega\Delta t$ is less than $\pi/2$, the time-history effect can, in the case of $k = 0.02$, be approximated by the effect of a constant time lag. The communication velocity that will produce this time lag Δt is $\bar{U}_B \approx 0.20\bar{U}_V$, where $\bar{U}_V \approx U_\infty$. At the seven times larger frequency $k = 0.14$ (where the time-history effect cannot be approximated by a single time lag), the time-history effect prevents the maximum camber generated at $\phi = 0$ to be experienced before the ends of the loop. This explains

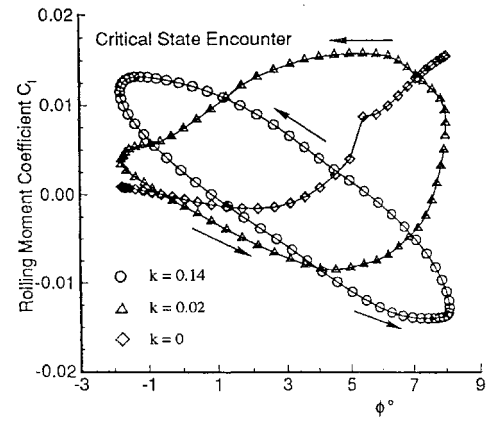

Fig. 8 $C_l(\phi)$ characteristics of 65-deg delta wing at -2 deg $\leq \phi \leq 8$ deg.[3]

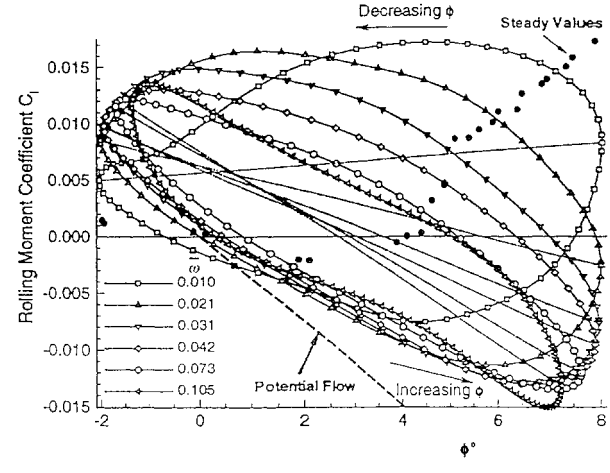

Fig. 9 $C_l(\phi)$ characteristics of 65-deg delta wing at -2 deg $\leq \phi \leq 8$ deg for varying reduced frequency.[30]

why the maximum width of the $C_l(\phi)$ loop is smaller for $k = 0.14$ than for $k = 0.02$. The unchanging width for $|\phi| \leq 3$ deg at $k = 0.14$ is believed to be mainly the result of the saturation effect discussed in Ref. 9, which could limit the maximum rate-induced camber from being significantly larger than for $k = 0.02$.

The results in Fig. 2 show that the time-lag effect on vortex breakdown for the rolling wing must be significantly larger than for a pitching delta wing[14] (Fig. 5), where the convection velocity for the camber effect on vortex breakdown was roughly 70% of that for the unburst vortex, $\bar{U}_B \approx 0.70\bar{U}_V$. For the rolling delta wing in Fig. 2, however, the experimental results give $\bar{U}_B \approx 0.20\bar{U}_V$. What is the reason for this big difference? It obviously must be related to the different flow mechanisms through which the camber effect is generated for pitching and rolling delta wings, a subject discussed earlier. For the pitching delta wing,[14] the generation of the camber is initiated at the apex and the influence on the vortex breakdown is realized mainly through downstream convection. In contrast, for the rolling delta wing, the generation of the camber is largely concentrated to the leading edge just upstream of the trailing edge. It must be communicated up to the apex before the downstream convection to the vortex breakdown can take place. The situation is somewhat similar to the upstream/downstream communication process existing in the

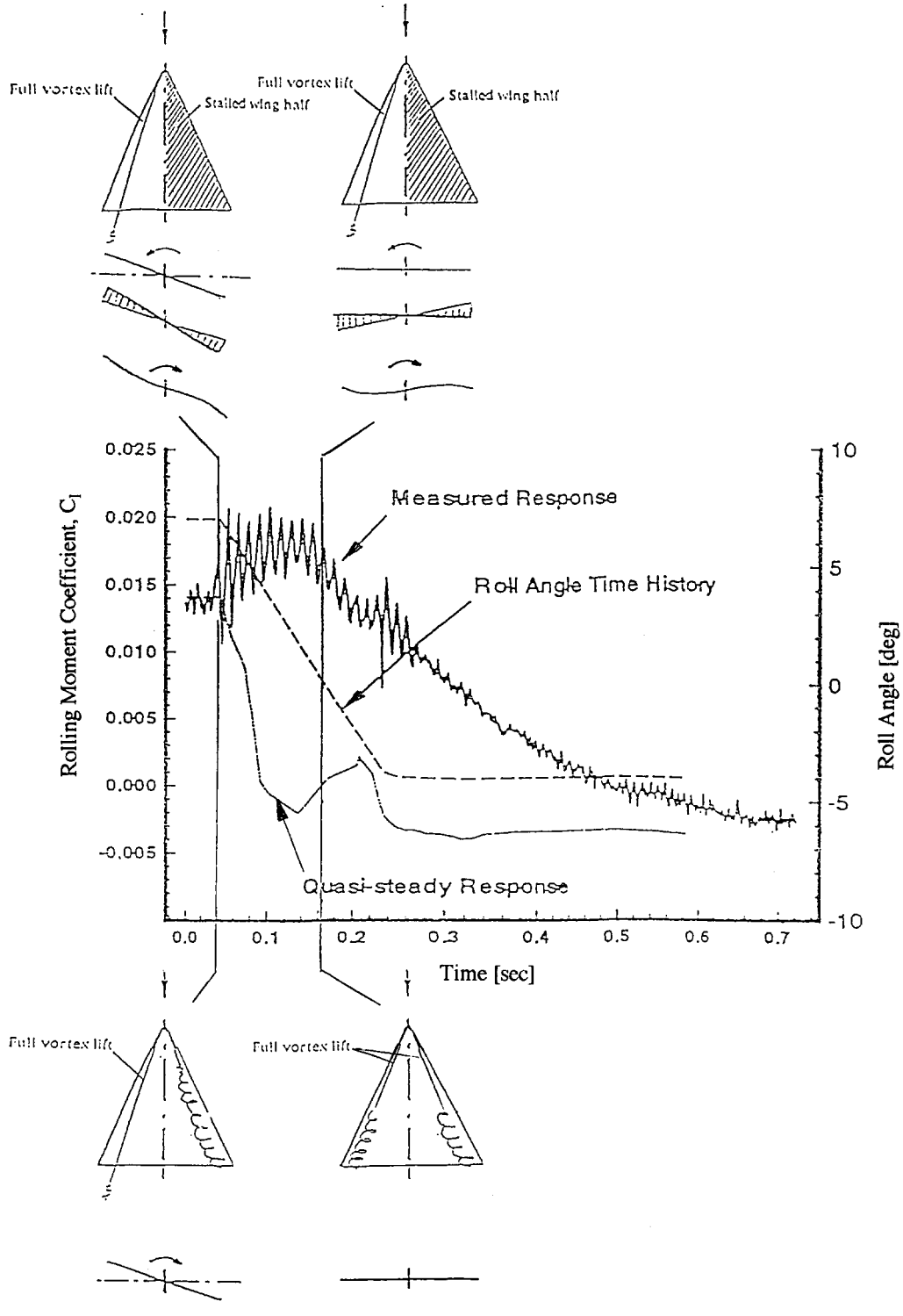

Fig. 10 Rolling-moment characteristics for rampwise change from $\phi = 7$ to -4 deg.[30]

case of dynamic sting support interference.[29] The velocity $\bar{U}_U$ for the communication of the rate-induced camber effect at the trailing edge to the apex can be determined as follows. When breakdown occurs at the trailing edge, the time required to communicate a change of flow conditions at the trailing edge to the apex can be expressed as $c/0.20\bar{U}_V$ or $c/\bar{U}_U + c/0.70\bar{U}_V$. That is, $\bar{U}_U$ is 28% of $\bar{U}_V$. This is very similar to the ratio between upstream and downstream communication velocities found in the case of dynamic sting interference.[29] In contrast to the difference in $\bar{U}_B$ between rolling and pitching delta wings, one does not expect any difference in $\bar{U}_V$. The change of the effective leading-edge sweep, caused by a change of the roll angle, should be convected downstream from the apex with $\bar{U}_V \approx U_\infty$, just as in the case of the pitch-induced change of angle of attack.[14]

The roll-rate-induced camber for $k = 0.02$, existing at $\phi \approx 4.2$ deg in Fig. 2 at the intersection $P(t)$ between dynamic and static $C_l(\phi)$ characteristics, was generated at $P(t - \Delta t)$. If $\phi(t - \Delta t) = 5$ deg, where $\dot{\phi} = 0$, the induced camber at $P(t)$ would be zero. However, for $\omega\Delta t = 40$ deg, one obtains $\phi(t - \Delta t) = \Delta\phi \sin(\pi/2 + \omega\Delta t) = \Delta\phi \cos 40 \text{ deg} = 3.85$ deg. That is, $\phi(t - \Delta t) < 4.2$ deg, and the roll-rate-induced camber at $P(t)$ was generated at $\phi = 3.85$ deg during the upstroke. Consequently, it is not zero, but generates a nonzero, negative rolling-moment contribution, which is experienced at $P(t)$. In regard to the effect of roll angle, the time lag is only 20% of that for the roll-rate effect, i.e., $\omega\Delta t = 8$ deg, giving $\phi(t - \Delta t) = 4.33$ deg. The corresponding positive contribution to the rolling moment was generated during the backstroke at $\phi = 4.33$ deg, balancing the roll-rate-induced negative C_l contribution to produce the needed zero net result at $\phi(t) = 4.2$ deg.

It is true that the time-lag effect on the roll-rate-induced camber could explain the increasing loop width when $|\phi|$ is increasing; going from the center, $\phi = 0$, toward the ends of the loops. However, another explanation is needed when $|\phi|$ is decreasing, going from the ends of the loop toward the center. As discussed earlier, the rate-induced camber generated a negative, statically stabilizing contribution to C_l at $P(t)$. Consequently, the maximum contribution to the loop width during the backstroke occurs when the rate-induced negative contribution to C_l at $P(t)$ has disappeared.

Comparing the experimental results for the 5-deg amplitude oscillations in Fig. 2 around $\phi_0 = 0$ with those in Fig. 8 around $\phi_0 = 3$ deg, one concludes that in the latter case, the encounter with the critical state at 5 deg $\leq \phi < 6$ deg (Ref. 8) changed the character of the dynamic $C_l(\phi)$ loops dramatically for $k = 0.02$, but not for $k = 0.14$ (compare Figs. 2 and 8). Figure 8 demonstrates the point made earlier in connection with Fig. 3, that the roll-rate-induced camber effect is expected to increase greatly when the vortex breakdown starts approaching the critical state more rapidly with increasing ϕ (Fig. 4). Thus, in the case of $k = 0.14$, the large roll-rate-induced camber effect has almost as strong an affect on $C_l(\phi)$ for no critical state encounter (Fig. 2) as for critical state encounter (Fig. 8). Recent experimental results[30] (Fig. 9) illustrate how fast the camber effect becomes dominant with increasing $\bar{\omega}$ for increasing ϕ during the upstroke, becoming saturated at $\bar{\omega} \approx 0.02$ ($k \approx 2\bar{\omega}$). In contrast, for decreasing ϕ during the backstroke, the reduced frequency $\bar{\omega}$ continues to have a significant effect throughout the tested frequency range. What causes this big difference between increasing and decreasing ϕ?

For $\bar{\omega} = 0.021$ in Fig. 9, $\omega\Delta t \approx 80 \text{ deg} < \pi/2$. Obviously, the roll-rate-induced residual camber at $\phi(t)$, which was shown earlier to be generated at $\phi(t - \Delta t) > 3$ deg during the upstroke, will produce a negative contribution to C_l of larger magnitude than for $\bar{\omega} = 0.010$ for two reasons: 1) the magnitude of the rate-induced camber for increasing ϕ during the upstroke is greater; and 2) the time lag is increased, permitting more of the camber-induced effect at $\phi(t - \Delta t)$ during the upstroke to be felt at $\phi(t)$ for decreasing ϕ during the backstroke, resulting in a lowering of the backstroke branch of the $C_l(\phi)$ loop. This time-history effect will increase with increasing $\bar{\omega}$, even after the rate-induced camber effect has become saturated during the upstroke. It is less obvious that the upstroke characteristics also are sensitive to the time-history effect. However, the negative $C_l(\phi)$ slope of the lines connecting the loop extremes at $\phi = -2$ and 8 deg in Fig. 9 increases in magnitude with increasing $\bar{\omega}$, even after the saturation of the camber effect. This is caused by the time-history effect illustrated by the time-lag effect $\omega\Delta t$ in Fig. 7, discussed earlier in connection with Fig. 2.

Recent experimental results[30] (Fig. 10) for a ϕ ramp from $\phi = 7$ to -4 deg, at $= \dot{\phi} = -0.003$, further illustrate the powerful time-history effect on the roll-rate-induced camber. According to Fig. 4, at $\phi = 7$ deg, the static vortex breakdown on the two wing halves is located as shown in the bottom sketch in Fig. 10. The top sketch

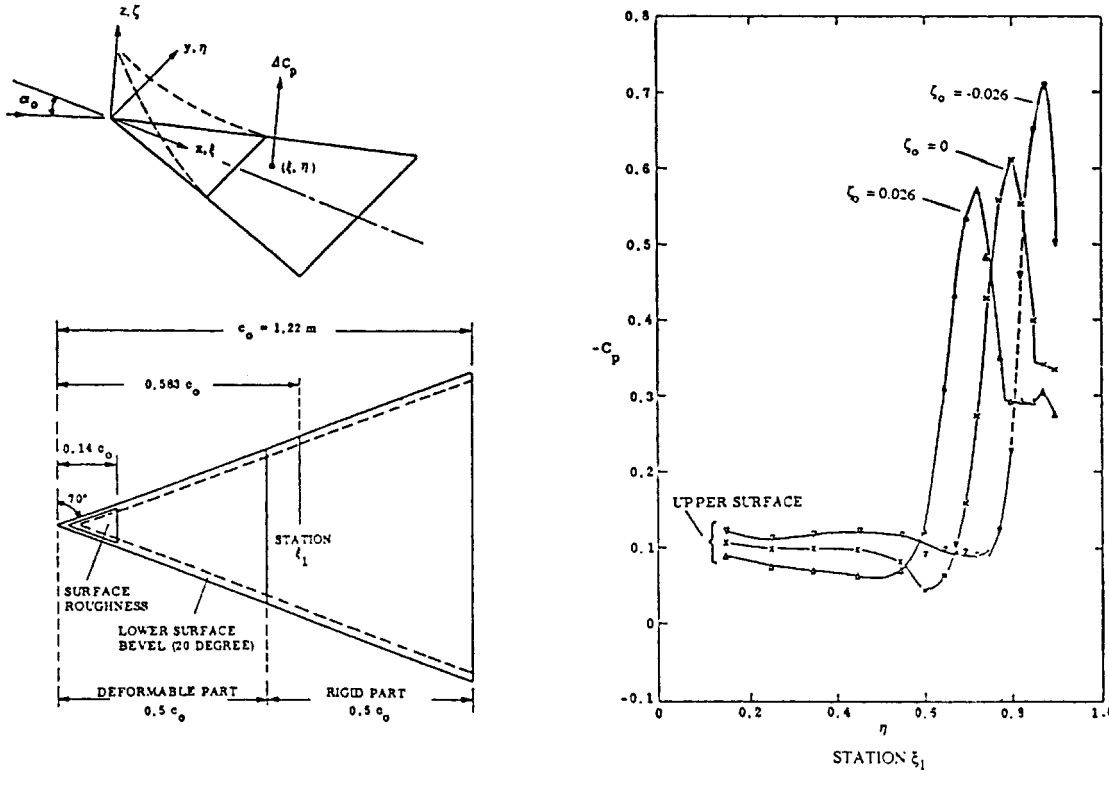

Fig. 11 Effect of longitudinal static camber on vortex-induced loads on a 70-deg delta wing.[23]

shows the effect of the roll-rate-induced camber (in the absence of time-history effects), causing the vortex breakdown to jump forward to the apex on the windward wing half, resulting in a loss of all its vortex-induced lift, producing an increase of the rolling moment. The rate-induced camber effect on the leeward, intact vortex would be to increase the vortex-induced lift and move it outboard[23] (Fig. 11), also increasing the rolling moment. Time-history effects cause the resulting increase of the rolling moment to be delayed until ϕ has decreased from 7 to ~5 deg. Because of the impact of initial conditions,[31] the dynamic flow characteristics and associated rolling moment change little when ϕ is decreased from 7 deg to 0 (top insets in Fig. 10). The long duration transient before the dynamic C_l has reached the static level, after the termination of the ϕ ramp at $\phi = -4$ deg, is in qualitative agreement with the transients observed for pitching delta wings.[31,32]

Although an increase of the rolling moment over its static value at $\phi = 5$ deg in Fig. 10 possibly "would occur with potential flow,"[30] the large increase observed in the present case is predominantly caused by the roll-rate-induced camber effect, which becomes extremely large when changing the roll angle at a nonzero rate through the ϕ range of the critical state, 7 deg $> \phi >$ 4 deg.[5,8] The large roll-rate-induced camber and associated large time-history effect discussed earlier help explain the sensitivity to the release angle of the early free-to-roll results.[7,33]

Conclusions

An analysis has been performed of the time-history effects on the measured unsteady aerodynamics of a sharp-edged 65-deg delta-wing-body configuration, describing large-amplitude/high-rate roll oscillations around an axis inclined 30 deg. It is shown that the observed large amplitude and rate effects on vortex breakdown can be explained when, in addition to the saturation of the roll-rate-induced camber effect, one considers that the rate-induced camber effect on the breakdown of leading-edge vortices is associated with a significantly larger time lag for rolling than for pitching delta wings.

References

[1]Hanff, E. S., and Jenkins, S. B., "Large-Amplitude High-Rate Roll Experiments on a Delta and Double-Delta Wing," AIAA Paper 90-0224, Jan. 1990.

[2]Herbst, W. B., "Dynamics of Air Combat," *Journal of Aircraft*, Vol. 20, No. 7, 1983, pp. 594–598.

[3]Hsia, A. H., Myatt, J. H., and Jenkins, J. E., "Nonlinear and Unsteady Aerodynamic Response of a Rolling 65° Delta Wing," AIAA Paper 93-3682, Aug. 1993.

[4]Ericsson, L. E., "Effect of Fuselage Geometry on Delta Wing Vortex Breakdown," *Journal of Aircraft*, Vol. 35, No. 6, 1998, pp. 898–904.

[5]Jobe, C. E., Hsia, A. H., Jenkins, J. E., and Addington, G. A., "Critical States and Flow Structure on a 65° Delta Wing Oscillating in Roll," *Journal of Aircraft*, Vol. 33, No. 2, 1996, pp. 347–352.

[6]Ericsson, L. E., "Analysis of Wind Tunnel Data Obtained in High-Rate Rolling Experiments with Slender Delta Wings," National Research Council, Inst. for Aerospace Research, CR-14, Canada, Aug.1991.

[7]Ericsson, L. E., and Hanff, E. S., "Further Analysis of High-Rate Rolling Experiments of a 65-Deg Delta Wing," *Journal of Aircraft*, Vol. 31, No. 6, 1994, pp. 1310–1317.

[8]Ericsson, L. E., "Flow Physics of Critical States for Rolling Delta Wings," *Journal of Aircraft*, Vol. 32, No. 3, 1995, pp. 603–610.

[9]Ericsson, L. E., "Difficulties in Predicting Vortex Breakdown Effects on a Rolling Delta Wing," *Journal of Aircraft*, Vol. 33, No. 3, 1996, pp. 477–484.

[10]Ericsson, L. E., "Vortex Breakdown Dynamics on Pitching Delta Wings," AIAA Paper 97-1777, June 1997.

[11]Huang, X. Z., and Hanff, E. S., "Roll Rate Induced Camber Effect on Delta Wing Leading-Edge Vortex Breakdown," AIAA Paper 95-1793, June 1995.

[12]Huang, X. Z., and Hanff, E. S., "Leading-Edge Vortex Behavior and Surface Flow Topology," Workshop III; Delta-Wing-Unsteady Aerodynamics and Modeling. AIAA Atmospheric Flight Mechanics Conf., Baltimore, MD, Aug. 1995 (Paper 2).

[13]Atta, R., and Rockwell, D., "Hysteresis of Vortex Development and Breakdown on an Oscillating Delta Wing," *AIAA Journal*, Vol. 25, No. 11, 1987, pp. 1512, 1513.

[14]Ericsson, L. E., "Pitch Rate Effects on Delta Wing Vortex Breakdown," *Journal of Aircraft*, Vol. 33, No. 3, 1996, pp. 639–642.

[15]Ericsson, L. E., "Pitch Rate Effects on Delta Wing Vortex Breakdown," *Journal of Aircraft*, (Errata) Vol. 34, No. 2, 1997, p. 264.

[16]Ericsson, L. E., and Reding, J. P., "Fluid Mechanics of Dynamic Stall, Part I, Unsteady Flow Concepts," *Journal of Fluids and Structures*, Vol. 2, No. 1, 1988, pp. 1–33.

[17]Ericsson, L. E., and Reding, J. P., "Approximate Nonlinear Slender Wing Aerodynamics," *Journal of Aircraft*, Vol. 14, No. 12, 1977, pp. 1197–1204.

[18]Woodgate, L., "Measurements of the Oscillating Pitching Moment Derivatives on a Delta Wing with Rounded Leading Edge in Incompressible Flow," Aeronautical Research Council, R&M 3628, Pt. 1, July 1968.

[19]Ericsson, L. E., and Reding, J. P., "Unsteady Aerodynamics of Slender Delta Wings at Large Angles of Attack," *Journal of Aircraft*, Vol. 12, No. 9, 1975, pp. 721–729.

[20]Ericsson, L. E., and King, H. H. C, "Effect of Cross-Sectional Geometry on Slender Wing Unsteady Aerodynamics," *Journal of Aircraft*, Vol. 30, No. 5, 1993, pp. 793–795.

[21]Ericsson, L. E., "Moving Wall Effects in Unsteady Flow," *Journal of Aircraft*, Vol. 25, No. 11, 1988, pp. 977–990.

[22]Ericsson, L. E., "Moving Wall Effects in Relation to Other Dynamic Stall Flow Mechanisms," *Journal of Aircraft*, Vol. 31, No. 6, 1994, pp. 1303–1309.

[23]Lambourne, N. C., Bryer, D. W., and Maybrey, J. F. M., "Pressure Measurements on a Model Delta Wing Undergoing Oscillatory Deformation," Aeronautical Research Council, National Physics Lab., Aero Rept. 1314, March 1970.

[24]Lambourne, N. C., and Bryer, D. W., "The Bursting of Leading-Edge Vortices—Some Observations and Discussion of the Phenomenon," Aeronautical Research Council, R&M 3282, April 1961.

[25]Tobak, M., Schiff, L. B., and Peterson, V. L., "Aerodynamics of Bodies of Revolution in Coning Motions," *AIAA Journal*, Vol. 7, No. 7, 1969, pp. 95–99.

[26]Ericsson, L. E., and Beyers, M. E., "Nonplanar Effects on Pitch Plane Dynamics," *Journal of Spacecraft and Rockets*, Vol. 27, No. 3, 1990, pp. 227–233.

[27]Ericsson, L. E., and Reding, J. P., *Asymmetric Flow Separation and Vortex Shedding on Bodies of Revolution*, Vol. 141, Progress in Astronautics and Aeronautics, AIAA, Washington, DC, 1992, pp. 391–452.

[28]Ericsson, L. E., and King, H. H. C., "Rapid Prediction of High-Alpha Unsteady Aerodynamics of Slender-Wing Aircraft," *Journal of Aircraft*, Vol. 29, No. 1, 1992, pp. 85–92.

[29]Reding, J. P., and Ericsson, L. E., "Dynamic Support Interference," *Journal of Spacecraft and Rockets*, Vol. 9, No. 7, 1972, pp. 547–553.

[30]Grismer, D. S., and Jenkins, J. E., "Critical-State Transients for a Rolling 65° Delta Wing," *Journal of Aircraft*, Vol. 34, No. 3, 1997, pp. 380–386.

[31]Ericsson, L. E., "Impact of Initial Conditions on the Effect of Pitch Rate on Delta Wing Vortex Breakdown," *Journal of Aircraft*, Vol. 34, No. 3, 1997, pp. 452–454.

[32]Reynolds, G. A., and Abtahi, A. A., "Instabilities in Leading-Edge Vortex Development," AIAA Paper 87-2424, Aug. 1987.

[33]Hanff, E. S., and Ericsson, L. E., "Multiple Roll Attractors of a Delta Wing at High Incidence," AGARD, CP-494, July 1991 (Paper 31).